Dominance of Linear 2-Coordination in Mercury Chemistry: Quasirelativistic and Nonrelativistic ab Initio Pseudopotential Study of $(HgX_2)_2$ (X = F, Cl, Br, I, H)

Martin Kaupp* and Hans Georg von Schnering

Max-Planck-Institut für Festkörperforschung, Heisenbergstrasse 1, D-70569 Stuttgart, Germany

Received August 19, 1993®

The preference of many solid mercury compounds for "molecular" structures with lower characteristic coordination numbers (frequently CN = 2) and lower boiling points than the corresponding zinc or cadmium species is due to relativistic effects. In particular, the relativistic increase of the mercury 6s-orbital ionization energies reduces the charge separation in and the intermolecular interactions between HgX_2 molecules containing electronegative substituents X. These are the major conclusions of extensive quasirelativistic and nonrelativistic ab initio pseudopotential Hartree–Fock and MP2 calculations on the dimeric systems $(HgX_2)_2$ (X = F, Cl, Br, I, H) and on the HgX_2 monomers. While quasirelativistic pseudopotential structure optimizations lead to weakly associated C_{2h} complexes of two almost linear HgX_2 units with Hg–X distances that are similar to those in the corresponding HgX_2 solid-state structures, use of a nonrelativistic Hg pseudopotential results in symmetrically bridged D_{2h} structures with far larger dimerization energies. Only $(HgH_2)_2$ exhibits slightly unsymmetrical bridging even with the nonrelativistic Hg pseudopotential. Natural population analyses (NPA) and the electron localization function (ELF) have been employed to rationalize the computed structural and thermochemical trends. While traditional explanations involving sd- or sp-hybridization arguments may have some bearing on the structures of HgH_2 or of organomercury compounds, electrostatic interactions and their relativistic reduction seem to be more important for the structural chemistry of mercury dihalides and similar compounds with electronegative ligands.

I. Introduction

The linear arrangement of two ligands around a central atom is observed in simple gas-phase or organic molecules, in organometallic compounds with bulky ligands, and also in solid-state structures of group 11 and group 12 compounds (e.g. $Ag(NH_3)_2^+$, $Au(PR_3)_2^+$, $HgCl_2$, etc.). However, linear 2-coordination is more predominant in the chemistry of mercury than for any other element. Frequently, two ligands form strong primary bonds to mercury in a linear arrangement, and additional bonding contacts with much longer distances lead to a $2+n$ coordination (n typically is 3–5).[1-5] This behavior has led to the introduction of the terms "characteristic coordination number" (number of strong covalent bonds) and "effective coordination number" (total number of bonding contacts within the sums of the ligand and metal van der Waals radii).[4] Examples for this coordination type in mercury chemistry are too numerous to be quoted here; overviews may be found in refs 3–5. The solid-state structure of $HgBr_2$ at ambient conditions[6] may serve as a typical example: Linear $HgBr_2$ units ("quasimolecules") with a Hg–Br distance of 2.48 Å are packed so that four secondary bonds to bromine atoms of neighboring molecules (at 3.23 Å) complete the metal environment to a strongly compressed octahedral 2 + 4 coordination (cf. Figure 1).

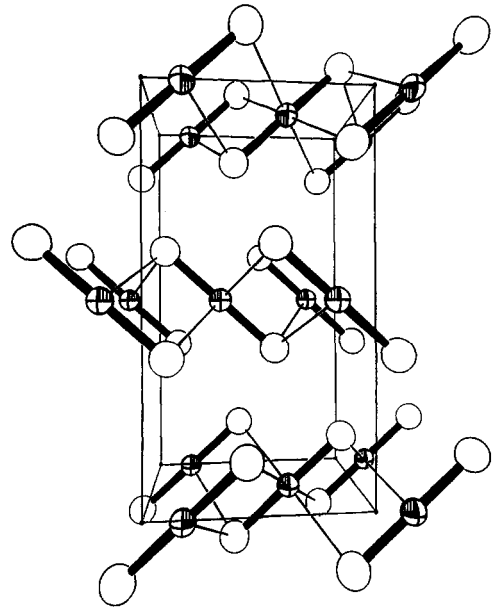

Figure 1. Schematic view of the solid-state structure of $HgBr_2$ (cf. ref 6). Octand-shaded circles represent the Hg atoms; open circles, the bromine atoms. Thick lines indicate the primary Hg–Br bonds (r = 2.48 Å); thin lines, the secondary contacts (r = 3.24 Å) and the unit cell boundaries.

In contrast, coordination number two is much rarer in the condensed-phase chemistry of the lighter group 12 metals Zn and Cd. It is mostly restricted to very bulky ligands or to organometallic species. Thus, e.g., in the solid state the dihalides exhibit ideal tetrahedral coordination for zinc and octahedral coordination for Cd, in prototypical layer structures (except for the difluorides which feature larger coordination numbers).[7]

The preference of mercury compounds for "molecular" structures with the characteristic coordination number two is

* Author to whom correspondence should be addressed. Temporary address from November 1993 through October 1994; Département de Chimie, Université de Montréal, C.P. 6128, Succ. A, Montréal, Québec H3C 3J7, Canada.

® Abstract published in *Advance ACS Abstracts*, April 15, 1994.

(1) (a) Cotton, F. A.; Wilkinson, G. *Advanced Inorganic Chemistry*, 5th ed.; Wiley: New York, 1988. (b) Greenwood, N. N.; Earnshaw, A. *Chemistry of the Elements*, Pergamon Press: Oxford, England, 1984. (c) Wells, A. F. *Structural Inorganic Chemistry*, 5th ed., Clarendon Press: Oxford, England, 1984.

(2) Aylett, B. J. In *Comprehensive Inorganic Chemistry*; Trotman-Dickenson, A. F., Ed.; Pergamon Press: Oxford, England, 1973; Vol. 3.

(3) Brodersen, K.; Hummel, H.-U. In *Comprehensive Coordination Chemistry*; Wilkinson, G., Ed.; Pergamon Press: Oxford, England, 1987; Vol. 5.

(4) Grdenic, D. *Q. Rev., Chem. Soc.* **1965**, *19*, 303.

(5) For further reviews on mercury coordination chemistry, see, e.g.: Dean, P. A. W. *Prog. Inorg. Chem.* **1978**, *24*, 109. Brodersen, K. *Comments Inorg. Chem.* **1981**, *1*, 207. Grdenic, D. In *Structural Studies of Molecular Biological Interest*, Dodson, G., Glusker, J. P., Sayre, D., Eds.; Clarendon Press: Oxford, England, 1981. Levason, W.; McAuliffe, C. A. In *The Chemistry of Mercury*; McAuliffe, C. A., Ed.; Macmillan: London, 1977.

(6) Verweel, H. J.; Bijvoet, J. M. *Z. Kristallogr.* **1931**, *77*, 122.

0020-1669/94/1333-2555$04.50/0

paralleled by far lower boiling points than those found for the corresponding Zn or Cd species. Thus, e.g., $HgBr_2$, $CdBr_2$ and $ZnBr_2$ boil at 319, 1136, and 697 °C, respectively.[2]

As a first step toward a better understanding of these pecularities of mercury coordination chemistry, we have now carried out ab initio pseudopotential studies on the dimers $(HgX_2)_2$ (X = H, F, Cl, Br, I). Dimers of this type (with X = halogen) have been identified by matrix-isolation IR and Raman spectroscopy.[8a] Halide-bridged dimers also exist in solution[8b] or even in the solid state[8c] when additional neutral ligands (e.g. phosphines or arsines) are present.

More importantly, the HgX_2 dimers represent the simplest models for more extended structures, and the moderate size of these molecular systems permits their study by accurate ab initio quantum-chemical methods. The molecular and electronic structures of the dimers and particularly the energetics of the dimerization process provide significant insights into the origin of the coordination preferences of HgX_2 and related compounds in the condensed phase.

It is well-known that relativistic effects are important for the chemical and physical properties of the heavy element mercury.[9-14] In particular, the relativistic contraction of the mercury 6s-orbital will render the charge transfer from mercury to electronegative ligands more difficult (for detailed explanations of relativistic effects on chemical properties of compounds containing heavy elements cf., e.g., refs 9–11). Thus, a major objective of the present study has been to find out to what extent relativistic effects are responsible for the low coordination numbers and for the low boiling points of many mercury compounds compared to their lighter group 12 congeners.

Some of the results for $(HgF_2)_2$ and HgF_2 have already been included in a previous study dealing mainly with mercury(IV) chemistry.[14] A few ab initio calculations are available for monomeric HgX_2.[12,13] No previous theoretical studies have been performed on the $(HgX_2)_2$ dimers.

II. Computational Methods

The HgX_2 monomers are known to be linear,[12,13,15] and structure optimizations at the Hartree–Fock (HF) and MP2 levels of theory[16] have been restricted to $D_{\infty h}$ symmetry. HF harmonic frequency calculations (cf. section III.D) confirm the linear monomer structures to be minima on the potential energy surfaces (PES). The dimers $(HgX_2)_2$ have been fully HF(MP2)-optimized within C_{2h} symmetry (cf. Figures 2–6). In cases where the HF optimization converged to a symmetrically bridged D_{2h} structure (in most calculations with a nonrelativistic pseudopotential), the MP2 calculation was restricted to D_{2h}. In cases with unsymmetrically bridged C_{2h} minima (e.g. in all quasirelativistic pseudopotential calculations), the symmetrical D_{2h} transition structure was also optimized for comparison. The nature of the stationary points on the (nonrelativistic and quasirelativistic pseudopotential) $(HgX_2)_2$ PES has been established by HF harmonic frequency calculations.

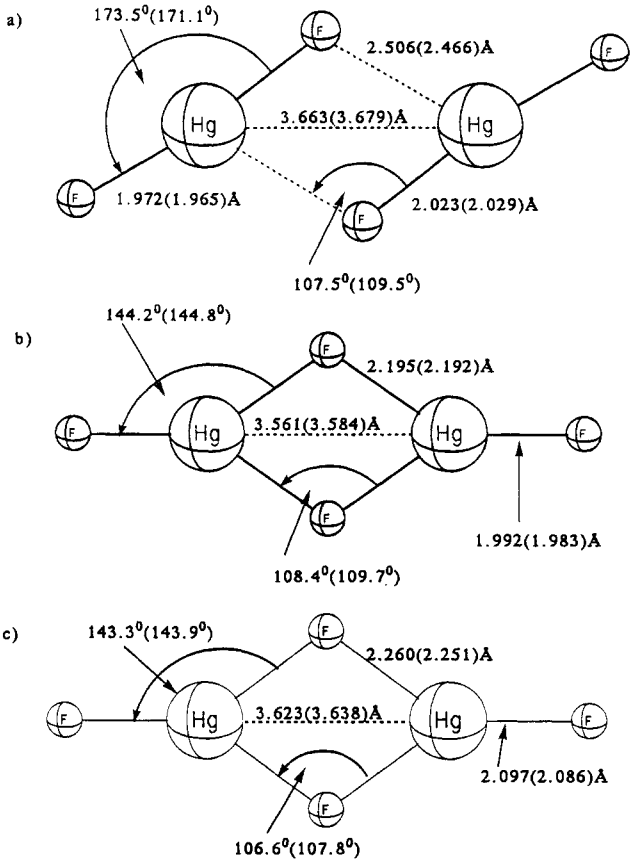

Figure 2. Results of structure optimizations for $(HgF_2)_2$: (a) full quasirelativistic MP2(HF) optimization in C_{2h} symmetry (minimum); (b) quasirelativistic HF optimization in D_{2h} symmetry (transition state); (c) nonrelativistic MP2(HF) optimization.

We employed the same quasirelativistic and nonrelativistic energy-adjusted 20-valence-electron pseudopotentials and (8s7p6d)/[6s5p3d] valence basis-sets for mercury[17] used in our recent computational studies of mercury(IV) chemistry.[14] For the halogen atoms, we used quasirelativistic 7-valence-electron pseudopotentials[18] and (5s5p1d)/[3s3p1d] valence basis sets[19] including diffuse functions. Note that the quasirelativistic pseudopotentials for the halogen atoms have been used even in comparative calculations with the nonrelativistic Hg pseudopotential. Thus, these calculations do consider scalar relativistic effects connected to the inner shells of the halogen atoms but not those for mercury. The relativistic contributions from the halogen core electrons to the molecular properties (even for the heavier halogens, Br and I) are expected to be less important than those for mercury[9] and have not been investigated in detail (although they are included implicity). A (4s1p)/[2s1p] basis[20] was employed for hydrogen.

(7) Prince, R. H. In *Comprehensive Coordination Chemistry*; Wilkinson, G., Ed.; Pergamon Press: Oxford, England, 1987; Vol. 5, pp 925–1046.
(8) (a) Givan, A.; Loewenschuss, A. *J. Chem. Phys.* **1976**, *64*, 1967. Given, A.; Loewenschuss, A. *J. Chem. Phys.* **1980**, *72*, 3809. (b) Cf., e.g.: Eliezer, I.; Algavish, G. *Inorg. Chim. Acta* **1974**, *9*, 257. Griffiths, T. R.; Anderson, R. A. *J. Chem. Soc., Faraday Trans. 2* **1979**, *75*, 957. Brill, T. B.; Hugus, Z. Z. *Inorg. Chem.* **1970**, *9*, 984. (c) Cf., e.g.: Schmidbaur, H.; Räthlein, K.-H. *Chem. Ber.* **1973**, *106*, 2491. Brodersen, K.; Palmer, R.; Breitinger, D. *Chem. Ber.* **1971**, *104*, 360. Bell, N. A.; Goldstein, M.; Jones, T.; Nowell, I. W. *J. Chem. Soc., Chem. Commun.* **1976**, 1039. Bell, N. A.; Dee, T. D.; Goldstein, M.; Nowell, I. W. *Inorg. Chim. Acta* **1983**, *70*, 215. Glasser, L. S. D.; Ingram, L.; King, M. G.; McQuillan, G. P. *J. Chem. Soc. A* **1969**, 2501.
(9) (a) Pyykkö, P. *Chem. Rev.* **1988**, *88*, 563. (b) Pyykkö, P.; Desclaux, J. P. *Acc. Chem. Res.* **1979**, *12*, 276.
(10) (a) Pitzer, K. S. *Acc. Chem. Res.* **1979**, *12*, 271. (b) Christiansen, P. A.; Ermler, W. C.; Pitzer, K. S. *Ann. Rev. Phys. Chem.* **1985**, *36*, 407.
(11) Norrby, L. J. *J. Chem. Educ.* **1991**, *60*, 110.
(12) Strömberg, D.; Gropen, O.; Wahlgren, U. *Chem. Phys.* **1989**, *133*, 207.
(13) (a) Schwerdtfeger, P.; Boyd, P. D. W.; Brienne, S.; McFeaters, J.; Dolg, M.; Liao, M.-S.; Schwarz, W. H. E. *Inorg. Chim. Acta* **1993**, *213*, 233. (b) Ziegler, T.; Snijders, J. G.; Baerends, E. J. *J. Chem. Phys.* **1981**, *74*, 1271. (c) Pyykkö, P. *J. Chem. Soc., Faraday Trans. 2* **1979**, *75*, 1256. (d) Wadt, W. R. *J. Chem. Phys.* **1980**, *72*, 2469. (e) Hay, P. J.; Wadt, W. R.; Kahn, L. R.; Bobrowicz, F. W. *J. Chem. Phys.* **1978**, *69*, 984.
(14) (a) Kaupp, M.; von Schnering, H. G. *Angew. Chem.* **1993**, *105*, 952; Kaupp, M.; von Schnering, H. G. *Angew. Chem., Int. Ed. Engl.* **1993**, *32*, 861. (b) Kaupp, M.; Dolg, M.; Stoll, H.; von Schnering, H. G. *Inorg. Chem.*, in press.
(15) Cf., e.g.: (a) Legay-Sommaire, N.; Legay, F. *Chem. Phys. Lett.* **1993**, *207*, 123. (b) Büchler, A.; Stauffer, J. L.; Klemperer, W. *J. Am. Chem. Soc.* **1964**, *86*, 4544.
(16) Explanations of standard levels of ab initio MO theory, such as the Hartree–Fock and MPn methods, may be found in: Hehre, W. J.; Radom, L.; Schleyer, P. v. R.; Pople, J. A. *Ab Initio Molecular Orbital Theory*; Wiley: New York, 1986.
(17) Andrae, D.; Häussermann, U.; Dolg, M.; Stoll, H.; Preuss, H. *Theor. Chim. Acta* **1990**, *77*, 123.
(18) Bergner, A.; Dolg, M.; Küchle, W.; Stoll, H.; Preuss, H. *Mol. Phys.* **1993**, *80*, 1431.
(19) (a) Kaupp, M.; Schleyer, P. v. R.; Stoll, H.; Preuss, H. *J. Am. Chem. Soc.* **1991**, *113*, 6012–6020. (b) *Gaussian Basis Sets for Molecular Calculations*; Huzinaga, S., Ed.; Elsevier: New York, 1984.
(20) Dunning, T. H.; Hay, P. J. In *Methods of Electronic Structure Theory*; Schaefer, H. F., III, Ed.; Modern Theoretical Chemistry, 3, Plenum Press: New York, 1977.

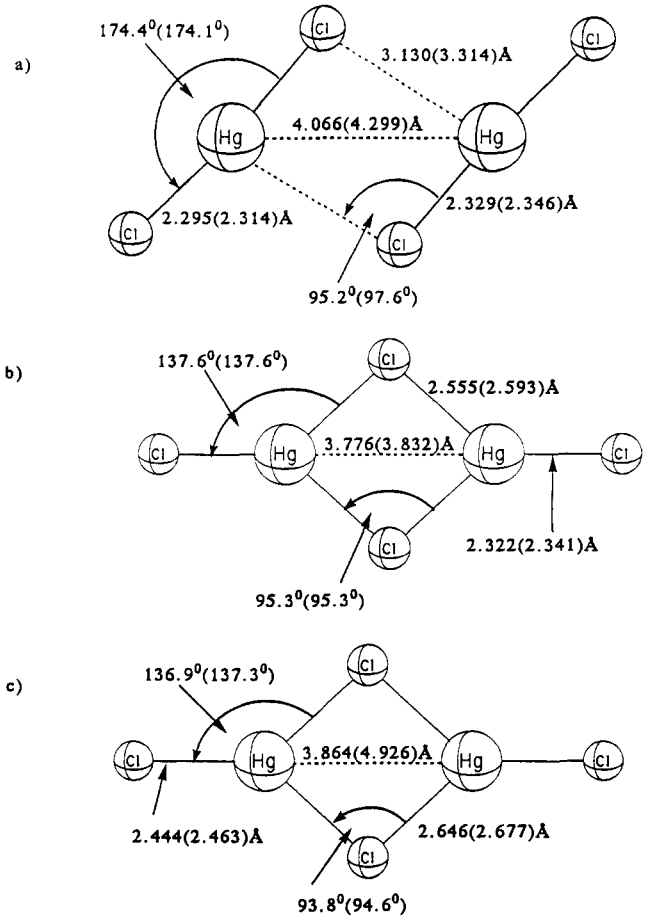

Figure 3. Results of structure optimizations for $(HgCl_2)_2$: (a) full quasirelativistic MP2(HF) optimization in C_{2h} symmetry (minimum); (b) quasirelativistic HF optimization in D_{2h} symmetry (transition state); (c) nonrelativistic MP2(HF) optimization.

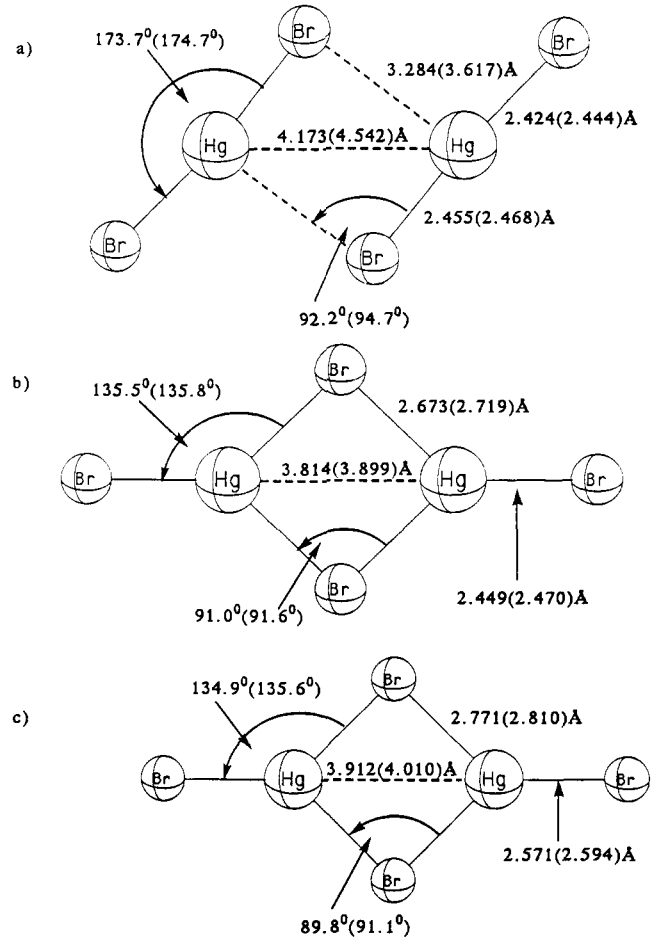

Figure 4. Results of structure optimizations for $(HgBr_2)_2$: (a) full quasirelativistic MP2(HF) optimization in C_{2h} symmetry (minimum); (b) quasirelativistic HF optimization in D_{2h} symmetry (transition state); (c) nonrelativistic MP2(HF) optimization.

The MP2 calculations correlated all electrons available outside the pseudopotential cores, including the 5s, 5p, and 5d shells on mercury. All calculations have been carried out with the Gaussian 92 program package.[21]

III. Results

After shortly discussing the HgX_2 monomers in section III.A, we will compare the structures of the dimers and the dimerization energies in sections III.B and III.C, respectively. Section III.D will provide harmonic vibrational frequencies for monomers and dimers. The electronic origin of the observed structural and energetic trends will be evaluated in section IV. In section V we will point out the direct relation between the present results for the HgX_2-dimers and the corresponding HgX_2 solid-state structures.

A. The HgX_2 Monomers. Table 1 gives the bond distances obtained for the linear HgX_2 monomers at the same theoretical levels used for the dimers, and experimentally. Table 2 lists MP2 atomization energies for the monomers.

Relativistic effects contract the Hg–X bonds by ca. 0.11–0.15 Å (cf. Table 1). This is similar to the contraction in closely related Au(I) compounds.[22] Due to the neglect of core-valence correlation, the quasirelativistic SCF bond lengths are somewhat longer (by ca. 0.04–0.07 Å) than the experimental (gas-phase) vales (cf. Table 1). As the MP2 calculations do not include basis functions with higher angular momentum than $l = 2$ to correlate the mercury 5d shell, the MP2 calculations still slightly (by ca. 0.02–0.06 Å) overestimate the bond distances. MP2 calculations for HgF_2 and $HgCl_2$ with extended ANO basis sets[23] give quite short distances (1.904 and 2.238 Å), whereas more elaborate ANO–QCISD calculations[23] yield 1.924 and 2.268 Å, respectively (the latter value is in excellent agreement with experiment, cf. Table 1). Thus, the performance of our limited basis-set MP2 optimizations is quite good, due to some error cancellation. This is important for the present study, as the size of the dimer systems discussed below does not yet allow the use of large-scale configuration interaction or coupled-cluster methods for structure optimizations.

The atomization energies given in Table 2 also benefit from a similar cancellation of errors inherent in the MP2 method with errors due to limited basis sets. Thus, the quasirelativistic MP2 atomization energies for HgF_2 and $HgCl_2$ are only ca. 50 kJ mol^{-1} larger than ANO–QCISD(T) results (which in turn may be slightly too low, cf. footnote *e* to Table 2).[23] We expect similar accuracy for X = Br and I. The MP2 atomization energy for HgH_2 (ca. 345 kJ mol^{-1}, Table 2) compares even more favorably with ANO–QCISD(T) results (351.7 kJ mol^{-1}).[23]

In spite of the relativistic bond contraction, all atomization energies given are reduced by relativistic effects. The bond

(21) Frisch, M. J.; Trucks, G. W.; Head-Gordon, M.; Gill, P. M. W.; Wong, M. W.; Foresman, J. B.; Johnson, B. G.; Schlegel, H. B.; Robb, M. A.; Replogle, E. S.; Gomperts, R.; Andres, J. L.; Raghavachari, K.; Binkley, J. S.; Gonzalez, C.; Martin, R. L.; Fox, D. I.; DeFrees, D. J.; Baker, J.; Stewart, J. P.; Pople, J. A. Gaussian 92, Revision A. Gaussian, Inc., Pittsburgh, PA, 1992.

(22) (a) Schwerdtfeger, P.; Boyd, P. D. W.; Brienne, S.; Burrell, A. K. *Inorg. Chem.* **1991**, *31*, 3481. (b) Schwerdtfeger, P. *J. Am. Chem. Soc.* **1989**, *111*, 7261. (c) Schwerdtfeger, P.; Dolg, M.; Schwarz, W. H. E.; Bowmaker, G. A.; Boyd, P. D. W. *J. Chem. Phys.* **1989**, *91*, 1762.

(23) Cf. ref 14 for the ANO–MP2 and ANO–QCI results on HgF_2. Calculations on $HgCl_2$ and HgH_2 used the pseudopotentials of refs 17 and 18 and the same extended ANO valence basis sets described in ref 14. A (7s2p)/[3s2p] hydrogen basis was employed.

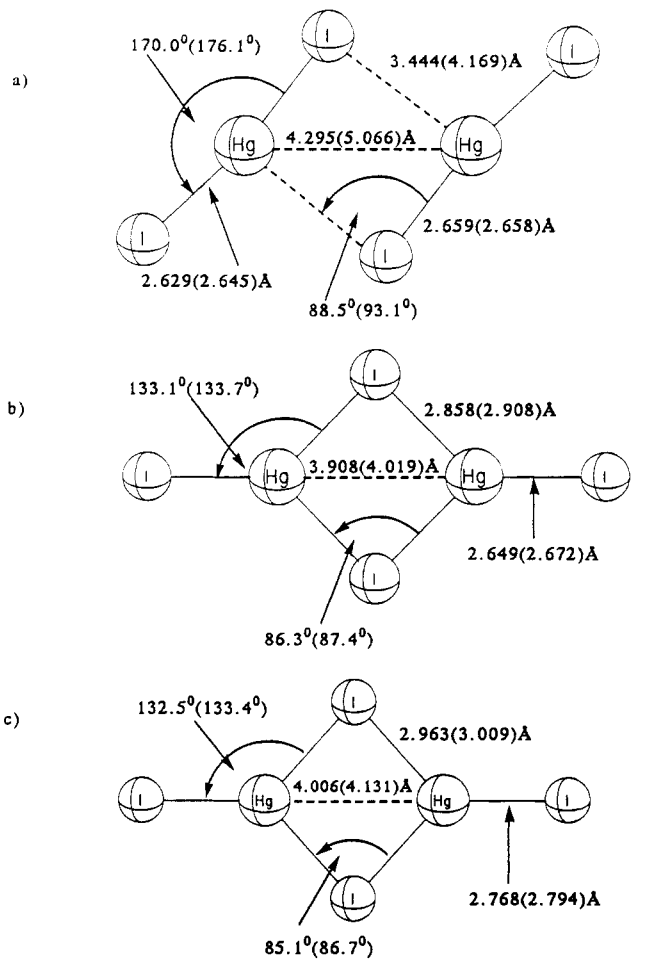

Figure 5. Results of structure optimizations for $(HgI_2)_2$: (a) Full quasirelativistic MP2(HF) optimization in C_{2h} symmetry (minimum); (b) quasirelativistic HF optimization in D_{2h} symmetry (transition state); (c) nonrelativistic MP2(HF) optimization.

destabilization due to scalar relativistic effects decreases along the series F > Cl > Br > I > H, in agreement with the decreasing bond ionicity: The relativistic increase in the first two ionization potentials of mercury destabilizes bonds to very electronegative elements, as discussed previously for gold(I) species[22] and for HgF_2.[14] Atomic spin–orbit (SO) coupling leads to a further reduction of the atomization energies for the heavier halides (molecular SO coupling has not been considered but is expected to be small[14]). Thus, the total relativistic destabilization of HgI_2 and HgF_2 is similar (Table 2, last column).

Our results for HgH_2, HgF_2, and $HgCl_2$ agree well with previous quasirelativistic all-electron or pseudopotential ab initio calculations,[12,13] both for the bond lengths and for the atomization energies (at comparable levels of treatment for electron correlation). This is also true for the magnitude of relativistic effects in these systems.

B. Structures of the HgX_2 Dimers. Figures 2–6 show the structures computed for the dimers $(HgX_2)_2$ (X = F, Cl, Br, I, H). The distances and angles obtained at the MP2 level are given, with the HF results in parentheses. Figures 2a–6a show the fully optimized C_{2h} structures obtained in the quasirelativistic pseudopotential calculations. These structures are all minima on the corresponding HF potential energy surfaces (PES). Figures 2b–6b give the quasirelativistic pseudopotential results for optimization in D_{2h} symmetry. These symmetrically bridged structures are all transition states (with one imaginary frequency). In contrast, optimization of the dihalide dimer structures in C_{2h} symmetry, using the nonrelativistic Hg pseudopotential, yielded symmetrically bridged D_{2h} minima (cf. Figures 2c–5c). Only $(HgH_2)_2$ exhibits an unsymmetrically bridged C_{2h} structure even

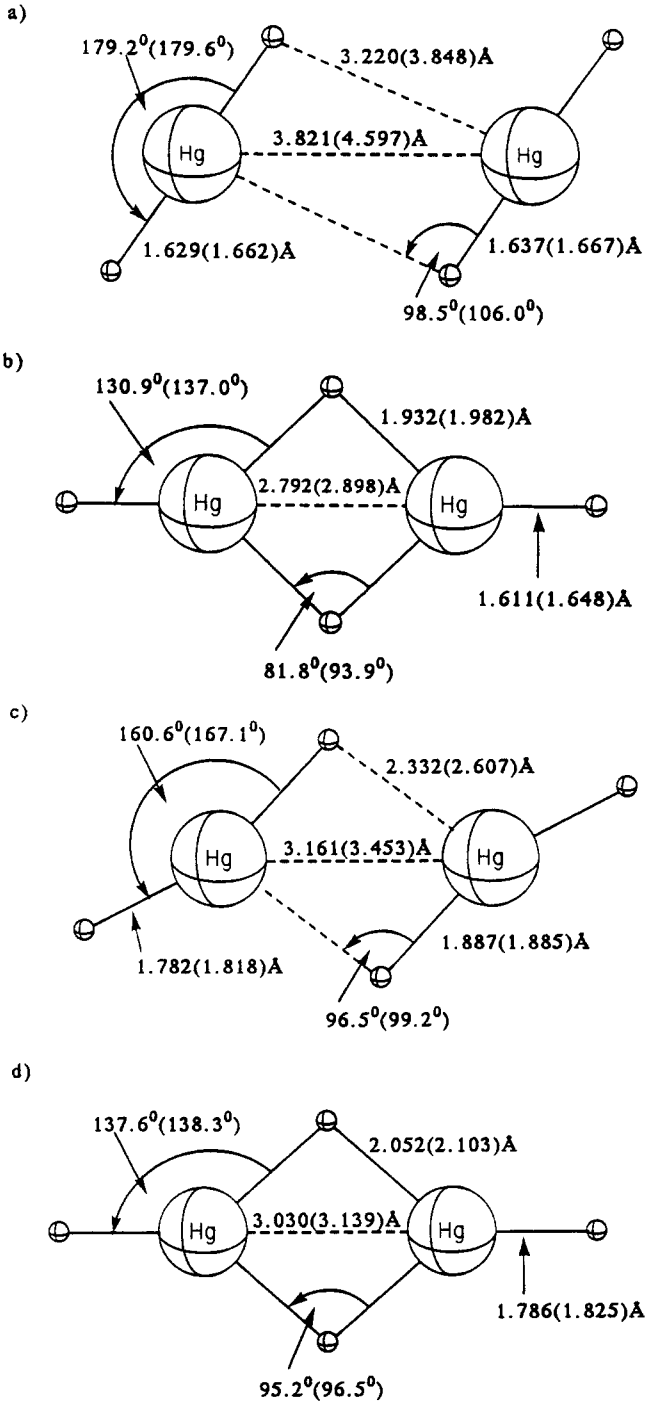

Figure 6. Results of structure optimizations for $(HgH_2)_2$: (a) full quasirelativistic MP2(HF) optimization in C_{2h} symmetry (minimum); (b) quasirelativistic HF optimization in D_{2h} symmetry (transition state); (c) nonrelativistic MP2(HF) optimization in C_{2h} symmetry (minimum); (d) nonrelativistic MP2(HF) optimization in D_{2h} symmetry (transition state).

in the nonrelativistic calculations (Figure 6c), with the symmetrical D_{2h} structure (Figure 6d) being a transition state.

The quasirelativistically optimized C_{2h} structures (Figures 2a–6a) all represent relatively loose complexes of almost linear HgX_2 fragments (at the MP2 level the smallest X_t–Hg–X_b angle is 170° for $(HgI_2)_2$, cf. Figure 5a). The lengthening of the Hg–X distances compared to the monomers is very small for the terminal Hg–X_t bonds (<0.01 Å at MP2), and still small for the primary Hg–X_b bonds (ca. 0.03–0.04 Å for the halides, only ca. 0.005 Å for X = H).

Interestingly, electron correlation generally decreases the separation of the two HgX_2 fragments (as measured by the

Table 1. Calculated MP2 (HF) and Experimental Hg–X Distances (Å) for HgX_2 (X = F, Cl, Br, I, H)

	calcd		exptl	
X	nr[a]	rel[b]	gas phase[c]	solid state[d]
F	2.079 (2.067)	1.965 (1.953)		8 × 2.46[e]
Cl	2.421 (2.441)	2.293 (2.313)	2.252[f]	2 × 2.25, 2 × 3.34, 2 × 3.63[g]
Br	2.546 (2.571)	2.421 (2.444)	2.40,[h] 2.44[i]	2 × 2.48, 4 × 3.23[j]
I	2.743 (2.769)	2.621 (2.645)	2.568[k]	2 × 2.62, 4 × 3.51[l]
H	1.782 (1.819)	1.632 (1.664)		

[a] Nonrelativistic pseudopotential results. [b] Quasirelativistic pseudopotential results. [c] The most recent electron diffraction or microwave spectroscopy data are given. [d] Shortest observed Hg–X contacts. [e] Eight equivalent nearest-neighbor contacts for mercury in an ionic fluorite structure, cf.: Ebert, F.; Woitinek, H. *Z. Allg. Anorg. Chem.* **1933**, *210*, 269. [f] Kashiwabara, K.; Konaka, S.; Kimura, M. *Bull. Chem. Soc. Jpn.* **1973**, *46*, 410. [g] Braekken, H.; Scholten, W. *Z. Kristallogr.* **1934**, *89*, 448. [h] Braune, H.; Knocke, S. *Z. Phys. Chem.* **1933**, *B23*, 163. [i] Gregg, A. H.; Hampson, G. C.; Jenkins, G. I.; Jones, P. L. F. *Trans. Faraday Soc.* **1937**, *33*, 852. [j] Braekken, H. *Z. Kristallogr.* **1932**, *81*, 152. [k] Spiridonov, V. P.; Gershikov, A. G.; Butaev, B. S. *J. Mol. Struct.* **1979**, *52*, 53. [l] β-HgI_2(yellow): Jeffrey, G. A.; Vlasse, M. *Inorg. Chem.* **1967**, *6*, 396.

Table 2. Comparison of Relativistic and Nonrelativistic MP2 Atomization Energies (kJ mol^{-1}) for HgX_2

X	nr[a]	rel[b]	ΔE_R[c]
F	706.0	529.7 (526.5)[d]	−176.3 (−179.5)[d]
Cl	578.5	434.9 (427.9)[d,e]	−143.6 (−150.6)[d]
Br	522.5	388.5 (359.1)[d]	−134.0 (−163.4)[d]
I	439.1	317.0 (256.7)[d]	−122.1 (−182.7)[d]
H	351.2	344.8	−6.4

[a] Nonrelativistic pseudopotential results. [b] Quasirelativistic pseudopotential results. [c] Relativistic effects on atomization energy. [d] Results in parentheses include atomic spin-orbit coupling corrections for the halogens. Experimental values have been used (cf.: Moore, C. E. *Atomic Energy Levels*; Circular National Bureau of Standards 467; National Bureau of Standards: Washington, DC, 1958). [e] An experimental value of ca. 448 kJ mol^{-1} has been given for $HgCl_2$ (cf.: Krasnov, K. B.; Timoshin, V. S.; Dailova, T. G.; Khandozhko, S. *Handbook of Molecular Constants of Inorganic Compounds*; Israeli Program for Scientific Translation: Jerusalem, 1970).

Table 3. Ratio of Long to Short Bridging Hg–X_b Distances in C_{2h} structures of $(HgX_2)_2$[a] and in Solid-State HgX_2 Structures[b]

X	MP2	HF	exptl[b]
F	1.24	1.22	1.0
Cl	1.34	1.41	1.48, 1.61
Br	1.34	1.47	1.30
I	1.30	1.57	1.34
H	1.97	2.31	

[a] Quasirelativistic pseudopotential results given (cf. Figures 2a–6a). Nonrelativistic MP2 (HF) results for $(HgH_2)_2$ are 1.24 (1.38). [b] Calculated from data in Table 1.

secondary Hg··X_b bond lengths or by the Hg··Hg distances), except for X = F where the MP2 calculations actually yield a larger separation. The contraction of the Hg··X_b and Hg··Hg distances by electron correlation increases considerably (from ca. 0.2 to ca. 0.7–0.8 Å) along the series X = Cl, Br, and I. The ratios of primary Hg–X_b to secondary Hg··X_b bond lengths are shown in Table 3. They are affected considerably by electron correlation for X = Br, I, and H. The MP2 calculations give similar ratios for X = Cl, Br, and I, a smaller one for X = F, and a very large one for X = H. These trends are also reflected in the dimerization energies (cf. section III.C).

Compared to the C_{2h} minima described above, the D_{2h} transition states (Figures 2b–6b) exhibit considerably shorter Hg··Hg distances. While this compression is relatively small for X = F (ca. 0.1 Å, Figure 2), it is larger for X = Cl, Br, and I (ca. 0.35–0.4 Å, Figures 3–5) and very large for X = H (ca. 1 Å, Figure 6a,b). For the dihalide dimers, the Hg–X_t bonds are slightly lengthened (ca. 0.02 Å) in going from C_{2h} to D_{2h} structures.

Table 4. MP2 (HF) Activation Energies (kJ mol^{-1}) for the Structural Transformation $C_{2h} \rightarrow (D_{2h})^{\ddagger} \rightarrow C_{2h}$ of $(HgX_2)_2$[a]

F	Cl	Br	I	H
21.7 (12.7)	34.2 (31.9)	30.9 (27.6)	11.7 (26.7)	95.5 (121.4)[a]

[a] The nonrelativistic MP2 (HF) result for $(HgH_2)_2$ is 2.0 (3.5) kJ mol^{-1}.

Table 5. Dimerization Energies (kJ mol^{-1}) for HgX_2

	MP2 (HF)			
X	E_{nr}[a]	E_{rel}[b]	$MP2_{cc}$[c]	Δ_r[d]
F	190.3 (207.6)	71.6 (79.9)	61.9	−118.7 (−127.7)
Cl	119.0 (104.1)	36.1 (18.5)	24.3	−82.9 (−85.6)
Br	106.4 (86.3)	33.7 (12.2)	22.3	−72.7 (−74.1)
I	99.4 (69.3)	31.2 (6.0)	23.6	−68.2 (−63.3)
H	29.1 (16.3)	8.7 (2.0)	3.7	−20.4 (−14.3)

[a] Nonrelativistic pseudopotential results. [b] Quasirelativistic pseudopotential results. [c] Quasirelativistic MP2 results including counterpoise corrections for BSSE. [d] Relativistic contributions to dimerization energies (without consideration of BSSE corrections).

Only $(HgH_2)_2$ exhibits a slight (ca. 0.02 Å) shortening. The large nuclear reorganization for the latter system is paralleled by a $C_{2h} \rightarrow D_{2h}$ MP2 activation barrier of almost 100 kJ mol^{-1} (cf. Table 4). In contrast, the energy required to deform the dihalide dimers to a symmetrically bridged D_{2h} structure are below 30 kJ mol^{-1}. We note that electron correlation, which increases this barrier somewhat for X = F, is unimportant for X = Cl and Br, but strongly reduces the barrier for X = I (Table 4). Interestingly, at the MP2 level the iodide has the smallest barrier, even less than the fluoride (cf. section V).

As may be inferred from Figures 2c–5c, relativistic effects are responsible for the formation of unsymmetrically bridged C_{2h} dihalide–dimer structures. The nonrelativistic calculations (i.e. calculations with a nonrelativistic Hg pseudopotential but with quasirelativistic halogen pseudopotentials) would predict all four systems to prefer a symmetrically bridged D_{2h} arrangement. The bond angles for these structures are similar to those computed for the quasirelativistic D_{2h} transition states, but the bond lengths differ considerably (cf. Figures 2b–5b vs Figures 2c–5c): Relativistic effects contract the Hg–X_t bonds by the same amounts as for the monomers (cf. Table 1, section III.A). The relativistic contraction of the bridging bonds is less pronounced, consistent with relativistically reduced inter-fragment interactions (cf. section III.C).

The change from a symmetrically bridged D_{2h} minimum structure with ca. 135° X_t–Hg–X_b angles in the nonrelativistic pseudopotential calculations (Figures 2c–5c) to C_{2h} structures with almost linear HgX_2 fragments in the calculations employing the quasirelativistic Hg pseudopotential (Figures 2a–5a) represents a remarkable influence of relativistic effects on bond angles. Large relativistic effects on bond angles previously have only been reported for some substituted plumbanes(IV).[24] The energies associated with the relativistic bond angle effects in $(HgX_2)_2$ are significant (cf. Tables 4 and 5 and section III.C), i.e. the large angle changes are not due to particularly shallow potential energy surfaces.

Only $(HgH_2)_2$ has an unsymmetrically bridged C_{2h} minimum even in calculations with the nonrelativistic Hg pseudopotential (cf. Figure 6c). However, the deviations from a symmetrical bridge are far smaller, and the bending of the HgH_2 fragments is larger than in the quasirelativistic calculations (cf. Figure 6a). Hence, the energy required to transform this arrangement into a symmetrical D_{2h} structure (Figure 6d) is very small (ca. 3.5 kJ mol^{-1} at MP2), in sharp contrast to the relativistic case (Table 4).

(24) (a) Kaupp, M.; Schleyer, P. v. R. *Angew. Chem.* **1992**, *104*, 1240; *Angew. Chem., Int. Ed. Engl.* **1992**, *31*, 1224. (b) Kaupp, M.; Schleyer, P. v. R. *J. Am. Chem. Soc.* **1993**, *115*, 1061–1073.

C. Dimerization Energies. Table 5 summarizes the MP2-(HF) dimerization energies for all five systems studied, both at the quasirelativistic and nonrelativistic Hg pseudopotential levels. The last column gives the scalar relativistic contributions Δ_r to the dimerization energies. In all cases Δ_r is negative, i.e. relativity considerably reduces the energy gained from dimerization of two HgX_2 molecules. The magnitude of relativistic effects decreases along the series X = F, Cl, Br, I, and H, with decreasing absolute dimerization energy. Thus, the relative reduction of the dimerization energy by relativity is very similar in all five systems, ca. 60–70%. Note that the scalar relativistic effects on the atomization energies of the monomers also decrease along this series of substituents (cf. section III.A and Table 1).

Electron correlation increases the dimerization energies for all systems except for $(HgF_2)_2$, both in the quasirelativistic and in the nonrelativistic calculations. This is consistent with the effect of electron correlation on the interfragment distances (cf. section III.B), i.e. with the increase of the Hg··Hg distance in Hg_2F_4 and the reduction of the Hg··Hg distances in the other four dimers. Nevertheless, HgF_2 exhibits by far the largest dimerization energy, ca. 70 kJ mol^{-1} compared to ca. 30–35 kJ mol^{-1} for the other halides and only ca. 9 kJ mol^{-1} for HgH_2. Also consistent with the structural results for the dihalide dimers, the electron correlation contributions are largest for HgI_2. Thus, while the HF results would suggest a decrease of the dimerization energies along the series X = Cl, Br, and I, the MP2 values are rather similar for the three heavier halides (Table 5).

The hydride system clearly is the most weakly bound aggregate (cf. Table 5), as suspected from the structure of the dimer (cf. Figure 6a and section III.B). The dimerization energy is below 10 kJ mol^{-1}, i.e. in the van der Waals range. In contrast, the nonrelativistic MP2 dimerization energy of ca. 30 kJ mol^{-1} is close to MP2 results for ZnH_2 (ca. 40 kJ mol^{-1}).[25]

It is known that energies for weak interactions calculated with limited basis sets suffer from basis-set superposition errors (BSSE), particularly at the correlated level. Therefore we have employed the counterpoise correction[26] to estimate the magnitude of the BSSE contributions to the MP2 dimerization energies. The resulting corrected energies $MP2_{cc}$ are also given in Table 5. Obviously, the BSSE contributions to the MP2 dimerization energies are significant (ca. 14, 33, 34, 24, and 57% for X = F, Cl, Br, I, and H, respectively). However, they do not affect the observed trends significantly.

D. Vibrational Frequencies. As Givan and Loewenschuss[8a] have assigned some of the IR and Raman frequencies observed in matrix-isolation studies of the mercury dihalides (in solid krypton matrices) to dimeric species, it is worthwhile to compare calculated and experimental frequencies of $(HgX_2)_2$ and HgX_2 (X = F, Cl, Br, I). Table 6 summarizes the data computed both for the HgX_2 monomers and for the dimers at the HF level. Experimental assignments are given in parentheses. Data for X = H have been included for comparison and also because the HgH_2 monomer has very recently been identified in matrix-isolation IR spectra.[15a]

The agreement between experimental and (unscaled) calculated frequencies for the monomers is excellent (generally better than 7%). This gives us confidence in the calculated results for the dimers as well. For the few stretching vibrations assigned to HgX_2 dimers by Givan and Loewenschuss,[8a] the agreement is also usually good. The experimentally observed Raman bands for the dimers probably should not be assigned to the highest-energy A_g mode but rather to the next highest one. This gives an agreement of better than 5% for X = Cl, Br, and I. Only for $(HgF_2)_2$ do the calculated values for both high-energy A_g modes deviate considerably from the experimental Raman value[8a] of 560 cm^{-1}. This casts some doubt on the assignment of this band. Possibly, matrix-site effects have to be taken into account.

Table 6. HF and Experimental[a] Harmonic Vibrational Frequencies ω (cm^{-1}) for HgX_2 and $(HgX_2)_2$

	HgX_2				
	X				
mode	F	Cl	Br	I	H
Π_u	159 (170)[b]	93	64	48	784 (770)[c]
Σ_g	577 (568)[b]	346 (353)[b]	215 (224)[b]	154 (164)[b]	2047
Σ_u	648 (642)[b]	399 (403)[b]	283 (293)[b]	227 (238)[b]	1933 (1900)[c]

	$(HgX_2)_2$				
	X				
mode	F	Cl	Br	I	H
A_u	51	21	11	7	59
A_g	83	32	22	13	11
A_g	86	54	35	23	157
B_u	91	44	24	13	23
B_g	126	86	62	48	778
A_u	168	96	66	50	784
B_u	209	97	64	47	778
A_g	276	122	74	51	790
A_g	478 (560)[b,d]	327 (345)[b]	208 (219)[b]	151 (158)[b]	1924
B_u	522	333	210	152	1929
B_u	606 (589)[b]	387	278 (286)[b]	225 (229)[b]	2045
A_g	611	387	276	224	2043

[a] Experimental data are given in parentheses. [b] Cf. ref 8a. [c] Cf. ref 15a. [d] This assignment is uncertain, cf. text.

While MP2 calculations for $(HgBr_2)_2$ and $(HgI_2)_2$ give frequencies slightly shifted from their HF values, they do not change the overall picture. Obviously, the interaction between the two monomers induces only a relatively small decrease in the frequencies of the monomer Hg–X stretching modes, except for HgF_2. Givan and Loewenschuss interpreted their observations with a centrosymmetric structure of the dimers and they assumed symmetrically bridged D_{2h} forms.[8a] Our calculations confirm the centrosymmetry, but show clearly that the dimers have unsymmetrically bridged C_{2h} structures (cf. section III.B and Figures 2a–6a).

IV. Electronic Origin of the Preference for Low Coordination Numbers

It is clear from the preceding sections that relativistic effects strongly reduce intermolecular interactions between HgX_2 molecules. This results in a preference for structures with linear "molecular" units, and low boiling points. However, what is the precise origin of this influence of relativistic effects on the aggregation behavior of mercury compounds?

Two possible reasons have been discussed in the literature to explain the predominance of linear 2-coordination in mercury chemistry. Nyholm[27] argued that the large 6s–6p gap prevents sp^2 or sp^3 hybridization and thus an extension of the primary coordination shell. We will call this *effect 1*. The alternative explanation of Orgel[28] (*effect 2*) invokes d–s hybridization due to a small 5d–6d gap. As discussed by Pyykkö and Desclaux,[9b] the relativistic contraction of the mercury 6s orbital increases both *effects 1* and *2* when compared with the lighter group 12 elements, Zn and Cd (the expansion of the 5d shell will additionally enhance *effect 2*).

Another possible explanation (*effect 3*), largely neglected up to now, should be considered: Due to the relativistic contraction and stabilization of the mercury 6s orbital, the charge separation in the HgX_2 monomers is reduced. This may be inferred from the metal charges and valence populations (natural population

(25) (a) Kaupp, M. Dissertation, Universität Erlangen-Nürnberg, 1992. (b) Kaupp, M.; von Schnering, H. G., submitted for publication in *Inorg. Chem.*

(26) Boys, S. F.; Bernardi, F. *Mol. Phys.* **1970**, *19*, 553.

(27) Nyholm, R. S. *Proc. Chem. Soc.* **1961**, 273.

(28) Orgel, L. E. *J. Chem. Soc.* **1958**, 4186.

Table 7. Comparison of NPA Metal Net Charges Q(Hg) and Net Valence Populations (6s, 6p, 5d) for HgX_2 Monomers from Nonrelativistic SCF (SCF_{nr}) and from Quasirelativistic SCF (SCF_{rel}) and MP2 ($MP2_{rel}$) Densities

	F	Cl	Br	I	H
			Q(Hg)		
SCF_{nr}	1.807	1.601	1.516	1.380	1.086
SCF_{rel}	1.593	1.325	1.221	1.065	0.906
$MP2_{rel}$	1.440	1.181	1.076	0.922	0.811
			6s Population		
SCF_{nr}	0.227	0.386	0.451	0.553	0.912
SCF_{rel}	0.558	0.720	0.789	0.900	1.161
$MP2_{rel}$	0.705	0.843	0.908	1.010	1.246
			6p Population		
SCF_{nr}	0.020	0.045	0.059	0.082	0.060
SCF_{rel}	0.024	0.050	0.064	0.087	0.049
$MP2_{rel}$	0.058	0.098	0.114	0.139	0.083
			5d Population		
SCF_{nr}	9.946	9.968	9.974	9.985	9.943
SCF_{rel}	9.822	9.902	9.924	9.947	9.885
$MP2_{rel}$	9.797	9.878	9.902	9.929	9.860

analysis, NPA,[29] was employed) obtained in nonrelativistic and quasirelativistic calculations on monomeric HgX_2 (see Table 7). Relativity reduces the NPA metal charges for the dihalides by ca. 0.2–0.3 electron (those for HgH_2 only by ca. 0.1 electron). As a result of this *effect 3*, charge–charge, charge–dipole, and dipole–dipole interactions between two HgX_2 monomers will also be reduced, and the formation of typically ionic, symmetrically bridged structures will be less favorable than for the corresponding Zn or Cd compounds. Note that atomic shell-structure expansion (particularly the lanthanide contraction) may also contribute to differences between Hg and its lighter congeners.

Due to the relativistic contraction of bonds to mercury (cf. section III.A) and to the slight relativistic expansion of the mercury 5d orbitals, repulsions between "core" 5d electrons and the valence density of a neighboring molecule may be increased by relativity. This could also disfavor intermolecular aggregation. We will call this *effect 4*.

Thus, we have to consider at least four effects which may be responsible for the peculiar coordination chemistry of mercury. All of them are enhanced by the influence of relativity, and it appears difficult if not impossible to quantify the relative importance of *effects 1–4*. However, some qualitative arguments, an examination of the data given in the preceding sections, and additional electron population data for the dimeric systems (Table 8) provide more insight. It turns out that considerations related to *effect 3* may be more important than the traditional explanations *1*[27] or *2*.[28]

Effect 1. In the dihalide systems, the mercury 6p-populations do not change appreciably in going from the monomers to the dimers, both in the quasirelativistic and in the nonrelativistic calculations (cf. Table 8). Even the 6p-populations in the symmetrically bridged D_{2h} dimer structures (transition states in the quasirelativistic calculations, minima in the nonrelativistic calculations, cf. Figures 2b,c–5b,c) are almost unchanged compared to the monomers. Thus, *effect 1* probably is of minor importance for the dihalides. Note that the p-populations are small even in the nonrelativistic calculations, and also in NPA analyses of various ZnX_2 compounds.[25] It should be noted that Mulliken population analyses (MPA)[30] yield larger p-populations than NPA. This is an artifact due to the even distribution of the overlap populations in MPA and has been discussed in detail by Reed, Weinstock, and Weinhold.[29]

The situation for HgH_2 is different: While the NPA p-populations in the extremely loose C_{2h} complex (quasirelativistic calculation, cf. Figure 6a) are unchanged from the monomers, the D_{2h} transition structure features considerably increased p-contributions (Table 8). Thus, in contrast to the rather ionic dihalides, the availability of metal p-orbitals may indeed be important for a genuine hydride-bridged structure. This is confirmed by an examination of atomic contributions to natural localized molecular orbitals (NLMO):[31] While contributions from metal p-orbitals to the Hg–H bonding orbitals in the monomer (or to the terminal Hg–H bonds in the dimer) are only ca. 2% of the metal s-contributions, the relative participation of metal 6p-orbitals is ca. 30% in the (much more ionic) bridging Hg–H bonds in the D_{2h} structure (both in the quasirelativistic and in the nonrelativistic calculations).

Thus, while the availability or unavailability of metal p-orbitals seems relatively unimportant for the more ionic dihalide systems, Nyholms original argument (*effect 1*)[27] may hold true for more covalent 2-electron–3-center hydride bridges, and possibly for alkyl or aryl bridges as well. This agrees with analyses of the dimerization of various alkaline-earth metal and zinc MX_2 compounds via different bridging groups,[25] and should not be attributed to relativistic effects.

Effect 2 vs Effect 4. As shown by the NPA populations at the bottom of Table 7, the depletion of the formally filled mercury $5d^{10}$-shell in the HgX_2 monomers follows the increasing polarization power of the anion X = I < Br < Cl < H < F. Is this due to an involvement of d-orbitals in bonding, as suggested by Orgel's original argument (*effect 2*),[28] or rather to a polarization (and compression) of the d-shell by the ligands, related to *effect 4*?

Table 9 gives the 5d/6s ratio of mercury atomic orbital contributions to the M-X bonding orbitals (2-center NLMOs[31]) in the HgX_2 monomers. The percentage of the total mercury AO contributions to the bonding NLMOs (indicating the degree of covalency of the MX bond) is also given. The d-contributions are slightly increased by relativity. However, even in the quasirelativistic calculations the degree of d-orbital participation in covalent bonding is generally small, except for HgH_2, where it is moderate. Thus, e.g., mercury 5d-orbital contributions are ca. 12% of the 6s-contributions in HgF_2 (quasirelativistic result), but due to the large ionicity the total mercury contributions (6s + 6p + 5d) make up only ca. 11% of the bonding orbital. While inclusion of electron correlation slightly increases covalency (cf. Table 7), the d/s ratios are almost unchanged.

Hence, only for HgH_2 the influence of sd-hybridization has to be considered. In going from two separated monomers to the symmetrically bridged D_{2h} transition state (cf. Figure 6b), the d-contributions to the terminal and to the bridging Hg–H bonds decrease from 14% to 6% and 9%, respectively, whereas the p-contributions increase (cf. above). Thus, in this case loss of sd-hybridization may slightly contribute to the reluctance to form a symmetrically bridged dimer. However, note that the actual involvement of mercury 5d-orbitals in bonding is small even for HgH_2, consistent with results for Hg–C bonding in a detailed study by DeKock et al. using density functional theory.[32]

Thus, the relatively large depletion of the mercury 5d-shell in the quasirelativistic calculations (cf. Table 7), e.g. for HgF_2, is not reflected in large d-contributions to covalent bonding. It may rather be the result of a polarization of the metal 5d-shell perpendicular to the bonding axis. Plots of the electron localization function (ELF)[33] for the monomeric HgX_2 molecules (cf. Figure 7 for HgF_2) support this view. Inclusion of the relativistic contraction of the mercury 6s orbital and the corresponding

(29) Reed, A. E.; Weinstock, R. B.; Weinhold, F. *J. Chem. Phys.* **1985**, *83*, 735.

(30) Mulliken, R. S. *J. Chem. Phys.* **1955**, *23*, 1833, 1841, 2338, 2343.

(31) (a) Reed, A. E.; Weinhold, F. *J. Chem. Phys.* **1985**, *83*, 1736. (b) Reed, A. E.; Curtiss, L. A.; Weinhold, F. *Chem. Rev.* **1988**, *88*, 899.

(32) DeKock, R. L.; Baerends, E. J.; Boerrigter, P. M.; Hengelmolen, R. *J. Am. Chem. Soc.* **1984**, *106*, 3387.

(33) Becke, A. D.; Edgecombe, K. E. *J. Chem. Phys.* **1990**, *92*, 5397. For the first implementations and tests of ELF, cf. Savin et al. (e.g. Savin, A.; Becke, A. D.; Flad, J.; Nesper, R.; Preuss, H.; von Schnering, H. G. *Angew. Chem.* **1991**, *103*, 421; *Angew. Chem., Int. Ed. Engl.* **1991**, *30*, 409).

Table 8. NPA Net Charges and Metal Valence Populations for the $(HgX_2)_2$ Dimers, and Changes Compared to the Separated Monomers (Numbers in Parentheses)[a]

	F	Cl	Br	I	H[b]
			C_{2h}(rel[c])		
Q(Hg)	1.667 (+0.074)	1.365 (+0.040)	1.254 (+0.033)	1.092 (+0.027)	0.914 (+0.008)
6s	0.448 (–0.110)	0.674 (–0.046)	0.754 (–0.035)	0.871 (–0.029)	1.151 (–0.010)
6p	0.023 (–0.001)	0.046 (–0.004)	0.059 (–0.005)	0.082 (–0.005)	0.049 (+0.000)
5d	9.859 (+0.037)	9.913 (+0.011)	9.932 (+0.008)	9.952 (+0.005)	9.885 (+0.000)
$Q(X_b)$	–0.863 (–0.069)	–0.704 (–0.041)	–0.647 (–0.036)	–0.564 (–0.031)	–0.471 (–0.018)
$Q(X_t)$	–0.804 (–0.008)	–0.660 (+0.003)	–0.607 (+0.004)	–0.528 (+0.005)	–0.443 (+0.010)
			D_{2h}(rel[c])		
Q(Hg)	1.726 (+0.136)	1.438 (+0.113)	1.316 (+0.095)	1.130 (+0.065)	1.002 (+0.096)
6s	0.339 (–0.219)	0.554 (–0.166)	0.651 (–0.138)	0.797 (–0.103)	0.981 (–0.180)
6p	0.024 (+0.000)	0.052 (+0.002)	0.067 (+0.003)	0.094 (+0.007)	0.085 (+0.036)
5d	9.907 (+0.085)	9.954 (+0.052)	9.965 (+0.041)	9.977 (+0.030)	9.935 (+0.050)
$Q(X_b)$	–0.906 (–0.110)	–0.760 (–0.097)	–0.693 (–0.082)	–0.589 (–0.056)	–0.617 (–0.054)
$Q(X_t)$	–0.821 (–0.025)	–0.679 (–0.016)	–0.622 (–0.011)	–0.542 (–0.009)	–0.385 (+0.068)
			D_{2h}(nr[d])		
Q(Hg)	1.865 (+0.062)	1.664 (+0.069)	1.572 (+0.059)	1.423 (+0.043)	1.214 (+0.140)
6s	0.141 (–0.086)	0.304 (–0.082)	0.379 (–0.072)	0.498 (–0.055)	0.738 (–0.174)
6p	0.018 (–0.002)	0.043 (–0.007)	0.057 (–0.002)	0.082 (+0.000)	0.075 (+0.015)
5d	9.974 (+0.028)	9.986 (+0.018)	9.989 (+0.025)	9.993 (+0.008)	9.961 (+0.018)
$Q(X_b)$	–0.948 (–0.047)	–0.847 (–0.049)	–0.798 (–0.042)	–0.714 (–0.024)	–0.692 (–0.149)
$Q(X_t)$	–0.916 (–0.015)	–0.816 (–0.018)	–0.774 (–0.018)	–0.709 (–0.019)	–0.523 (+0.020)

[a] Analysis of SCF densities at MP2-optimized structures. [b] Nonrelativistic pseudopotential results for Hg_2H_4 in C_{2h} symmetry are as follows: Q(Hg) = 1.183 (+0.097), 6s = 0.788 (–0.124), 6p = 0.069 (+0.009), 5d = 9.961 (+0.018), $Q(H_b)$ = –0.660 (–0.117), and $Q(H_t)$ = –0.523 (+0.020). [c] Quasirelativistic Hg pseudopotential used. [d] Nonrelativistic Hg pseudopotential used.

Table 9. d/s Ratio and Approximate Weight[a] of Mercury NAO Contributions to M–X Bonding NLMOs in HgX_2[b]

	rel[c]		nr[d]	
X	d/s ratio	wt, %	d/s ratio	wt, %
F	0.12	11	0.03	5
Cl	0.08	19	0.02	10
Br	0.06	22	0.02	12
I	0.05	27	0.02	15
H	0.14	36	0.05	28

[a] Total share of mercury NAOs in the Hg–X bonding NLMO. [b] SCF density analyzed. [c] Quasirelativistic Hg pseudopotential. [d] Nonrelativistic Hg pseudopotential.

expansion of the 5d orbital increases the polarization of the mercury $5s^25p^65d^{10}$ core-shell significantly (Figure 7b). Further support comes from the smaller 5d occupancies in the natural population analysis (NPA) of the MP2 densities compared to the SCF densities of HgX_2 (bottom rows in Table 7), as inclusion of electron correlation is expected to improve the description of the d-shell polarization.

In going from the separated monomers to the dimers (particularly to the tight symmetrically-bridged D_{2h} structures) the metal 5d-shell with experience further repulsive interactions (*effect 4*). These will tend to compensate the polarization shown in Figure 7b, resulting in an apparent increase of the d-occupation (cf. Table 8). Notably, this increase is largest for X = F, i.e. in the system with the largest electrostatic interactions. However, it will be difficult to quantify the energetic effect of this repulsion. An ELF visualization of these 5d-shell polarization effects in $(HgF_2)_2$ is shown in Figure 8 (parts a–c give the ELF for the quasirelativistic C_{2h} and D_{2h} and the nonrelativistic D_{2h} structures, respectively). The considerable deformation of the mercury $5d^{10}$-core in the D_{2h} transition state (Figure 8b) is particularly notable (compare with Figure 8c for the nonrelativistic result).

Effect 3. We have already mentioned above that the relativistic contraction of the mercury 6s-shell decreases the charge separation in the monomers (Table 7) and thus reduces the low-order multipole interactions between two monomeric units (*effect 3*).

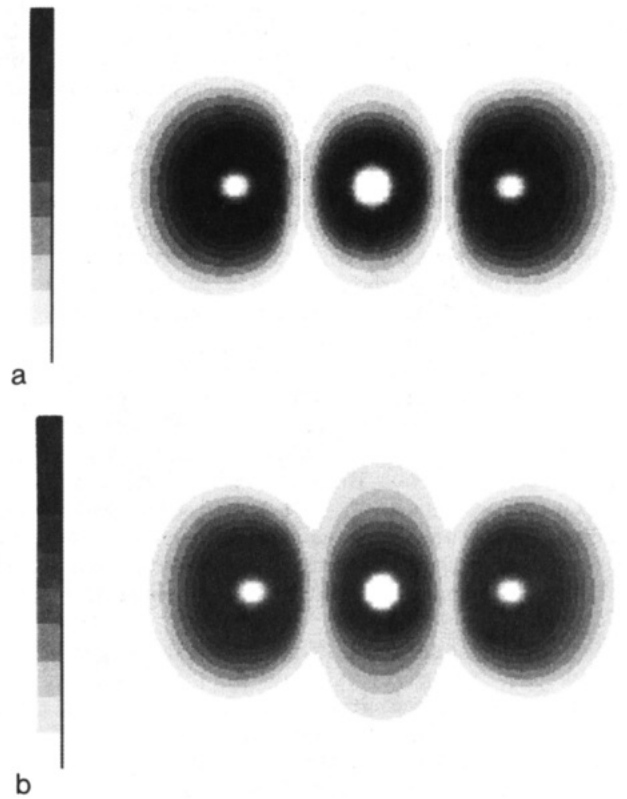

Figure 7. Graphical representation of the electron localization function (ELF, cf. ref 33) for HgF_2. The HF densities have been analyzed for the MP2 optimized structures. The grey scale employed is shown on the left side. Dark areas indicate high electron localization (ELF close to 1), lighter areas indicate low localization (ELF close to 0). The fluorine atoms are located to the left and to the right; the mercury atom is located in the center. Low ELF values (white spots) at the nuclear positions reflect the use of pseudopotentials for the inner core electrons. Key: (a) nonrelativistic pseudopotential for Hg; (b) quasirelativistic pseudopotential for Hg.

The electrostatic character of the interactions, as opposed to typical electron-pair donor/electron-pair acceptor interactions, is supported by the observed *increase* of the charges on the metals and on the bridging ligands compared to the separated monomers (cf. Table 8). This *increase in bond ionicity* upon aggregation is

(34) MPA assigns larger negative charges to the terminal compared to the bridging ligands for X = Cl, Br, and I. This may be an artifact of MPA due to the presence of diffuse functions both on the metal and on the halogen atoms.

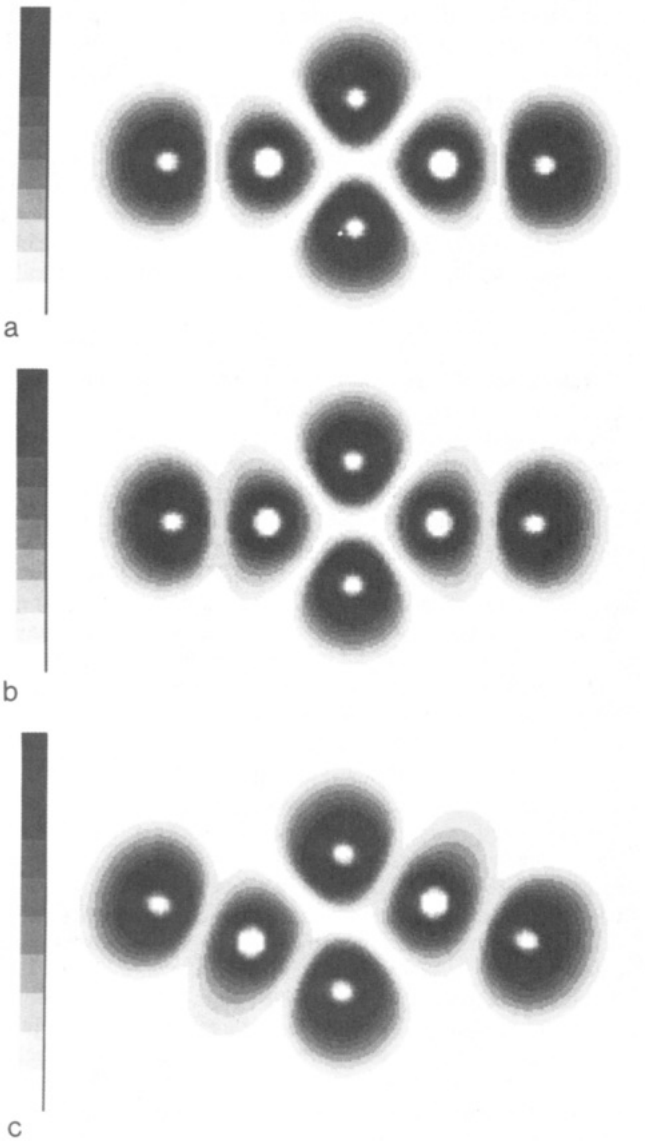

Figure 8. Graphical representation of the electron localization function (ELF, cf. ref 33) for $(HgF_2)_2$. See comments to Figure 7. Key: (a) nonrelativistic Hg pseudopotential, D_{2h} minimum; (b) quasirelativistic Hg pseudopotential, D_{2h} transition state; (c) quasirelativistic Hg pseudopotential, C_{2h} minimum.

most pronounced for the symmetrically bridged D_{2h} transition states, and largest for X = F. It should be noted that this increase of metal charge upon dimerization is observed for all species, irrespective of the type of density used (MP2 or HF) and irrespective of the type of population analysis, NPA or MPA.[34] A similar increase of the metal charge in going from monomeric to dimeric species has been computed for various group 2 and Zn MX_2 compounds,[25] for group 14 dihydrides and difluorides,[35] and also for a number of LiX species.[36] This effect seems to be quite general for systems where the dimerization is driven mainly be interactions between partial dipoles (incomplete charge separation in the monomers), rather than only by Coulombic forces (at the completely ionic limit, e.g. for LiF[36]) or by an acid/base charge-transfer mechanism.

The implications for the aggregation of the HgX_2 monomers are obvious: Electronegative ligands from neighboring molecules remove charge from the metal. However, due to the large 6s ionization potential (increased by relativity), any further charge withdrawal from the already positively charged metal will be expensive energetically. Thus, the relativistic increase in the mercury 6s ionization potential reduces not only the binding energies in the HgX_2 monomers (cf. section III.A. and Table 2) but also the energy gained from interactions with additional electronegative ligands. Preliminary computational results on the anions HgX_3^- and HgX_4^{2-} indicate that the same factors may be responsible for the reluctance of mercury to form simple symmetric complex anions with electronegative ligands.[37]

(35) (a) Trinquier, G. *J. Am. Chem. Soc.* **1990**, *112*, 2130. (b) Trinquier, G.; Barthelat, J.-C. *J. Am. Chem. Soc.* **1990**, *112*, 9121.
(36) Cf., e.g.: Sannigrahi, A. B.; Kar, T. *THEOCHEM* **1988**, *49*, 149.

Table 10. Comparison of MP2 HgX_2 Dimerization Energies (kJ mol^{-1}) to Those Obtained in a Simple Point Charge Model[a]

X	MP2	point charge model
F	71.6	142.4
Cl	36.1	31.3
Br	33.7	18.4
I	31.2	10.9
H	8.7	−23.1[b]

[a] NPA partial charges for Hg and X_b from HF densities and MP2 optimized Hg··X_b, Hg··Hg, and X_b··X_b distances have been used for the point charge model. [b] Unbound.

The above introduction of *effect 3* was based on the assumption that the Hg and X charges (and thus the interacting dipoles) will remain unchanged upon dimerization. The increase in the charge separation apparent from Table 8 puts even more emphasis on the importance of electrostatic interactions and on their reduction due to relativistic effects. The adequacy of the electrostatic arguments may also be confirmed by comparing the dimerization energies obtained from a simple electrostatic model with the ab initio values: The rough estimates of the dimerization energies given in Table 10 have been obtained by using the NPA charges (Table 8) and bond distances (Figures 2a–6a) for the MP2-optimized C_{2h} structures of M_2X_4 in a simple point-charge model. The results agree well with the trends of the ab initio values and also with their order of magnitude, except for X = H.

Interpretation of Electron-Correlation Contributions to Dimerization. As discussed in Section III, except for HgF_2, electron correlation favors the dimerization of the HgX_2 molecules studied; i.e., the inter-fragment separations are smaller and the dimerization energies are larger at MP2 compared to HF. Moreover, the importance of the correlation contributions increases considerably along the series X = Cl, Br, and I. This suggests that the driving force for dimerization gradually changes from lighter to heavier halides.

Comparison of natural bond orbital (NBO)[31b] analyses of the HF and MP2 densities, e.g. for $(HgI_2)_2$, gives no evidence for any significant influence of electron correlation on the charge transfer between the monomeric units. More likely, aggregation via iodine bridges involves larger dispersion-type interactions than for the lighter halides. Large contributions from electron correlation to interactions between soft acids and soft bases have been observed previously.[38] Repulsions between two bridging halides or between bridging halide and Hg core shells could also be responsible for larger electron correlation contributions in the heavier dihalide dimers. Notably, electron correlation contributions also give $(HgI_2)_2$ the smallest $C_{2h} \rightarrow D_{2h}$ activation barrier (cf. section III.B., Table 4) of the dihalide dimers.

The slight reduction of the dimerization energy of HgF_2 by electron correlation (cf. Table 5) may be due to the reduced charge separation in the correlated density (cf. Table 7) and supports the largely electrostatic mechanism of dimerization (cf. above).

V. Comparison to HgX_2 Solid-State Structures

To emphasize the generality of the conclusions drawn from our computational results for the $(HgX_2)_2$ dimers, it is worthwhile to compare structural and energetic results to experimental data

(37) Kaupp, M. Unpublished results.
(38) Chattarai, P. K.; Kaupp, M.; Schleyer, P.v.R. Unpublished results.

Table 11. Comparison of Experimental Melting Points T_m (°C), Boiling Points T_b (°C), and Vaporization Enthalpies ΔH_{vap}^{298} (kJ mol^{-1}) for the Mercury Dihalides[a] and Computed HgX_2 Dimerization Energies E_{dim}[b] (kJ mol^{-1})

species	T_m	T_b	ΔH_{vap}^{298}	E_{dim}[b]
HgF_2	645 (dec)	647	92.0	61.9
$HgCl_2$	277	304	58.9	24.3
$HgBr_2$	241	319	59.2	22.3
HgI_2	257	354	59.2	23.6

[a] Cf. ref 2. [b] Counterpoise-corrected MP2 results; cf. Table 5.

for the HgX_2 solid-state systems. We will not consider solid-state structures featuring true halide-bridged dimers $(HgX_2L)_2$ (L = PR_3, AsR_3).[8c] In these species, the influence of the neutral coligands L on structures and bonding is too large[8c] for a direct comparison to the "naked" dimers of the present study.

In Table 11 the melting and boiling temperatures, T_m and T_b, and the vaporization enthalpies, ΔH_{vap}, of bulk HgX_2 are compared to the counterpoise-corrected MP2 dimerization energies (cf. Table 5). The relatively high boiling point and vaporization enthalpy of HgF_2 is consistent with the large dimerization energy. The vaporization energies for the other three halides are almost the same; so are the calculated dimerization energies, but only when electron correlation contributions are included (cf. Table 5)!

As the only binary mercury compound exhibiting an extended, typically ionic (CaF_2-type) lattice (cf. Table 1), solid HgF_2 plays a special role. The dimer (cf. Figure 2a) does not exhibit a symmetrically bridged structure. However, the dimerization energy (Table 5) obviously is considerably larger and the ratio of long to short bridging HgX_b bond lengths is smaller than for the other four systems (cf. Table 3). This is due to the large charge separation present in the monomer (cf. Table 7). The approach of only one neighboring molecule apparently does not suffice to remove the digonal bond directionality in HgF_2 (in the nonrelativistic calculations it would, cf. Figure 2c), but the combined electrostatic forces in the extended lattice do.

At the MP2 level, the longer Hg–Cl bridging distance in $(HgCl_2)_2$ (cf. Figure 3a) is considerably shorter than the secondary distances in the solid state (cf. Table 1). This may be due either to some overestimate of electron correlation contributions by the MP2 method (or possibly to basis-set superposition errors, cf. Section III.C), or rather to the fact that four such contacts are present for each molecular unit in the solid state (Table 1). The results for the dimer emphasize the largely molecular nature of solid $HgCl_2$. The MP2 secondary Hg–X distances for $(HgBr_2)_2$ and $(HgI_2)_2$ (Figures 4 and 5a) agree better with the secondary contacts in the solid state (cf. Table 1), while the HF values are considerably too long. This indicates that electron correlation is essential to describe the association of the heavier halides but also suggests that the MP2 calculations on the dimer systems model the bonding in the HgX_2 solid-state structures quite well.

The most stable solid-state structure of HgI_2 at room temperature, red α-HgI_2, is not a molecular one but exhibits layers of edge-sharing HgI_4 tetrahedra (with Hg–I distances of ca. 2.78 Å).[39] The $HgBr_2$-analogous brucite-type structure of yellow β-HgI_2 (cf. Table 1 for the Hg–I distances) is metastable below 126 °C but stable above this temperature. Thus, it appears that the transition from a molecular structure with a "characteristic coordination number" (CCN) of 2 to a polymeric structure with a CCN of four is easier for the iodide than for the chloride or bromide. We have an indication for such a trend in our results on $(HgX_2)_2$: The MP2 barrier for transformation of the unsymmetrically bridged minimum C_{2h} structure to the symmetrically bridged D_{2h} transition state is only ca. 11 kJ mol^{-1} for X = I but ca. 30–35 kJ mol^{-1} for X = Cl and Br. As the HF barriers for the three systems are rather similar, it seems likely that dispersion-type interactions involving the rather polarizable iodide ions are responsible for the easier deformation of the iodide. Preliminary computational results on anionic halide complexes HgX_3^- and HgX_4^{2-} support this reasoning.[37]

No solid-state structural data are available for the elusive compound HgH_2. However, our computational results for $(HgH_2)_2$ (Figure 6a, Table 5) suggest solid HgH_2 to exhibit isolated molecules with low intermolecular interactions, similar to the group 12 dialkyl compounds.[1] The low aggregation energy may also contribute to the known high reactivity of HgH_2.[40]

VI. Conclusions

Relativistic effects reduce the energy gained from the aggregation of two HgX_2 molecules (X = Hal, H) by ca. 60–70% (cf. section III.C.). While calculations using a nonrelativistic Hg pseudopotential would predict symmetrical D_{2h} structures for the mercury dihalide dimers, the quasirelativistic calculations show that the dimers are relatively loose C_{2h} complexes of two almost linear HgX_2 molecules (section III.B.). Preliminary calculations on ZnX_2 or CdX_2 dimers (X = F, Cl, H) indicate symmetrically-bridged D_{2h} structures (except for Cd_2H_4) and larger dimerization energies for these species.[25] Thus, many of the differences between the coordination behavior of mercury and its lighter homologues may indeed be traced back to the relativistic kinematics of electron motion near the high Z nucleus (Z = 80) of the heavy element mercury.[9-11,41]

The extrapolation of our results for the HgX_2 dimers to the condensed-phase chemistry of mercury seems straightforward. The computed structural trends for $(HgX_2)_2$ (at the quasirelativistic level) are closely analogous to those, e.g., in the corresponding solid-state HgX_2 compounds (section V). For X = Cl, Br, I, even the computed primary and secondary Hg-X distances for the dimers compare well with solid-state data. The calculated relativistic reduction of the dimerization energies is doubtlessly related to the low boiling points of HgX_2 compounds compared to their ZnX_2 or CdX_2 analogues (of course explicit computational comparisons of the bulk systems are nevertheless desirable[25b]). It is conceivable that relativistically reduced aggregation and solvation energies of HgX_2 compounds may also be responsible for the unique competitiveness of Hg_2X_2 species in the condensed phase. We are presently studying this question by ab initio calculations on suitable model systems.

A combination of population analyses, ELF plots, and other data has provided additional insights into the origins of mercury's preference for low coordination numbers in compounds with electronegative ligands. While traditional hybridization arguments[27,28] may be useful for ligands like X = H or X = alkyl, electrostatic factors seem to be more important for compounds with quite electronegative groups such as, e.g., the halides: The relativistic contraction of the mercury 6s-orbital reduces the charge separation between metal and ligands and thus also decreases the low-order multipole interactions between the HgX_2 molecules. Indeed, the population analyses indicate further charge withdrawal from the metal upon aggregation. Due to the relativistically increased mercury 6s-ionization potential this is a less favorable process than for the analogous Zn or Cd compounds.

Finally, the comparisons of quasirelativistically and nonrelativistically optimized structures for $(HgX_2)_2$ have provided remarkable examples for large relativistic effects on bond angles.

Acknowledgment. We thank Dr. L. Schröder for help with the preparation of the figures and Dr. F. Wagner for providing his program for the display of ELF.

(39) Jeffrey, G. A.; Vlasse, M. *Inorg. Chem.* **1967**, *6*, 396.

(40) Wiberg, E.; Henle, W. *Z. Naturforsch. B* **1951**, *6b*, 461.

(41) Schwarz, W. H. E. *Phys. Scr.* **1987**, *36*, 403. Schwarz, W. H. E. In *Theoretical Models of Chemical Bonding*; Maksic, B., Ed.; Springer: Berlin, 1990; Vol. 2, p 593.